Angewandte Chemie
Eine Zeitschrift der Gesellschaft Deutscher Chemiker

Supporting Information

Mechanical Activation Drastically Accelerates Amide Bond Hydrolysis, Matching Enzyme Activity

*Michael F. Pill, Allan L. L. East, Dominik Marx, Martin K. Beyer, and Hauke Clausen-Schaumann**

anie_201902752_sm_miscellaneous_information.pdf

Content:

Methods:

Reagents. As substrate surfaces, highly ordered pyrolytic graphite (HOPG) (H.O.P.G., Mosaizitaet 3.5°, Plano) or Diamond Like Carbon (DLC) (Ge Windows AR/DLC 7-14 microns; UQG Optics) were used. Cantilevers with a DLC coated surface with a nominal spring constant of 200 mN m^{-1} (BudgetSensors, ContDLC), or custom made high density carbon tips (Nanotools) on Au-coated SiN cantilevers with a nominal spring constant of 100 mN m^{-1} (OMCL-TR400PSA Olympus,) or 60 mN m^{-1} (NPG-10, Bruker) were used. Carboxymethylated amylose (CMA) was purchased from Sigma-Aldrich and Santa Cruz Biotechnology. Polymer bound 1-(3-dimethylaminopropyl)-3-ethylcarbodiimide (EDC), N-hydroxysuccinimide (NHS), phosphate buffered saline (PBS; buffer composed of 137 mM NaCl, 10 mM Na_2HPO_4, 3 mM KCl, and 2 mM KH_2PO_4, pH 7.4 at T = 25 °C), allylamine, allyl alcohol, hydrochloric acid, α-tocopherol, and adipic acid were all purchased from Sigma-Aldrich. Ethanol (EtOH) (absolute GR for analysis) was obtained from Merck. α,ω-Bis-carboxy poylethylene glycol (bis-carboxy-PEG) with a PEG molecular weight of 3 kDa was purchased from Rapp Polymere.

AFM Tip and Surface Functionalization. After carbon substrates and AFM cantilevers were cleaned in EtOH, they were submerged in 10 % allylamine and 90 % EtOH solution inside a custom-made reaction chamber. The chamber was equipped with a UV-light source, emitting the mercury spectrum with the primary wave length at 254 nm (UV PenRay, Ultra-Violet Products Ltd, Cambridge, UK, Model 11SC-1), to induce radicals on carbon substrate and carbon AFM tip and allow allylamine to bind (cf. Fig. S1). At a lamp current of 15 mA AC and a distance of approx. 2 cm from the substrate, the light intensity at 254 nm was 4.4 mW cm^{-2}. To reduce side reactions with oxygen, such as the formation of peroxides, the reaction was carried out under a nitrogen atmosphere. After 5 hours under UV irradiation, residual radicals were quenched with

α-tocopherol treatment for 5 minutes, followed by rinsing with EtOH. For the control experiments where the amide bond was replaced by an ester bond, a solution with 10 % allyl alcohol instead of allylamine was used.

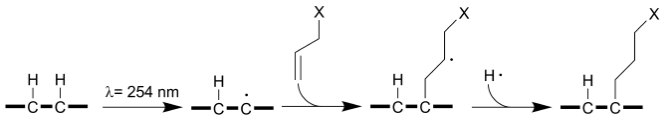

Figure S1. Functionalization of carbon substrate and carbon cantilever tip with an allylamine or allyl alcohol surface linker. X stands for the amine or the alcohol group.

AFM Experiments. CMA was activated with EDC and NHS and covalently anchored on the amine functionalized carbon substrates via multiple amide bonds, as described before for amine functionalized glass:[1] CMA, EDC and NHS were dissolved in PBS to a final concentrations of 10 mg mL^{-1} CMA, 25 mg mL^{-1} EDC, and 1 mg mL^{-1} NHS. This solution of activated CMA was transferred to the amine functionalized carbon substrate, for amide bond formation. After a reaction time of 10 min, the substrate was rinsed with PBS in order to remove non-covalently bound CMA from the substrate. The CMA coated substrate was then transferred to the AFM and covered with PBS. Prior to the force clamp experiments, cantilever spring constant was determined using the thermal noise method,[2] where the mean value of three independent calibrations was used. The gains of the force feedback loop were adjusted. For experiments above 21°C, the temperature was set to the target value using a custom-built resistance heating stage monitored with a Pt100/1 temperature sensor (Bürklin). After thermal equilibrium had been reached, the CMA covered substrate was approached with a maximum contact force of 0.25 nN and the tip was permitted to rest at the surface for 3 s, to allow amide bond formation between tip and activated CMA. The tip was then retracted at a velocity of 5 μm s^{-1}. When a CMA molecule

was attached to the AFM tip, it was stretched until the predefined clamp force was reached, and from then on, the survival time of the bond was recorded. All successful force curves were checked for the characteristic plateau of CMA between 300 and 400 pN,[1a] which indicates that only one single molecule is probed. We assume that the allylamide used for tip and surface functionalization undergoes oligomerization, which gives sufficient conformational flexibility for the newly formed amide bond to relax relative to the force vector. The fact that we observe mono-exponential decay kinetics for all forces except 0.7 nN supports this interpretation. All experiments were carried out using the Force RampDesigner software of a NanoWizard I AFM (JPK Instruments). Unless stated otherwise, experiments were carried out at room temperature (21°C) and neutral pH (7.4) in PBS buffer.

Control Experiments. Controls where CMA was replaced by adipic acid or by bis-carboxy-PEG were carried out identically, except for replacing CMA with adipic acid or bis-carboxy-PEG, respectively (Cf. Fig. S2 and Fig. S3).

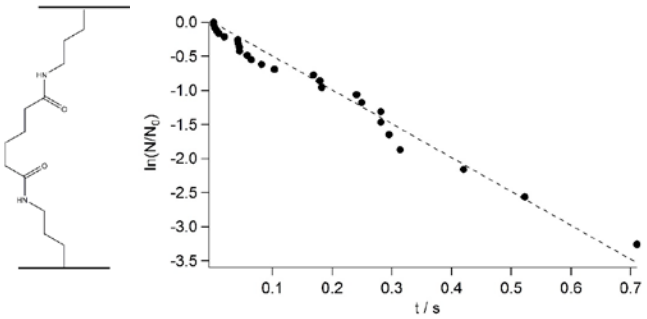

Figure S2. To rule out that a bond in the CMA spacer is breaking instead of the amide bond, we replaced the CMA spacer by adipic acid (left). Number of intact bonds vs. time (right) of the force clamp experiments with adipic acid as spacer. The reaction rate constant, evaluated with a first-order rate law (dotted line), is k = (4.97 ± 0.12) s^{-1}, corresponding to τ = (0.201 ± 0.005)s at room temperature and 0.8 nN clamp force, compared to (5.86 ± 0.90) s^{-1} and τ = (0.171 ± 0.026) s with CMA.

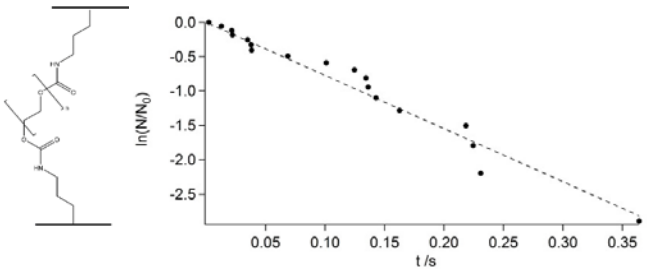

Figure S3. Molecular setup (left) and umber of intact bonds vs. time (right) of force clamp experiments were the CMA spacer was replaced by bis-carboxy-PEG. Experiments were carried out at room temperature and 1.0 nN clamp force. The resulting reaction rate constant is k = (7.73 ± 0.25) s^{-1}, corresponding to τ = (0.129 ± 0.004) s, compared to k = (6.89 ± 0.85) s^{-1} or τ = (0.145 ± 0.018) s with CMA at room temperature and 1.0 nN.

To replace the amide bond by an ester bond, allyl alcohol functionalized substrates and AFM tips were incubated for 10 min with a 10 mg mL^{-1} CMA solution at pH 2 (the pH-value was adjusted with hydrochloric acid), before they were thoroughly rinsed and transferred to the AFM (all at pH 2), as described by Schmidt *et al.*[3]

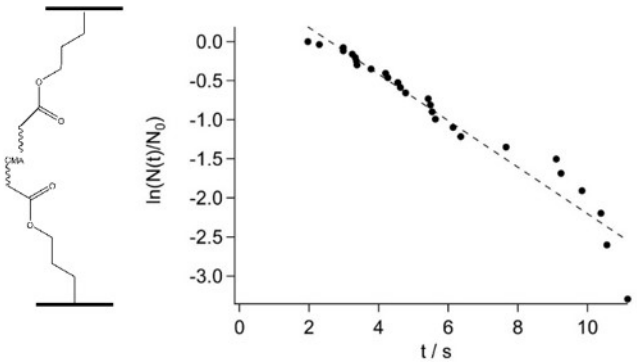

Figure S4. Molecular setup (left) and number of intact bonds vs. time (right) of CMA linked to allyl alcohol functionalized substrate and AFM tip via ester bonds. Experiments were carried out at room temperature and 0.8 nN clamp force. The resulting reaction rate constant, evaluated with a first-order rate law (dotted line), is k = (0.21 ± 0.02) s^{-1} or τ = (4.8 ± 0.45) s

Data analysis. To determine the force dependent reaction rate constants in Fig. 1E, we fitted a first order rate law (exponential decay) to each data set, using the maximum likelihood

estimation (MLE), as shown in Fig. 1D and described before.[3b] To determine the force and temperature dependent reaction rate constants in Fig. 3, as well as force dependent activation energies, we applied a global MLE fit to all data points, using the Bell model, as described in detail by Schmidt et al.[3b] These global fit parameters together with the Bell model were also used to extrapolate force dependent reaction rate constants and activation energies to F = 0 nN, as described by Schmidt et al.[3b] The fit algorithms were implemented in Matlab (R2017b, MathWorks). Error margins were derived from the experimental data using the MLE algorithm as described by Schmidt et al.[3b]

Computational Model: Energies. First-principles molecule energies were computed with the Gaussian09 program package [4] on the University of Regina supercomputer Dextrose. We report electronic single-point MP2/TZVP [5] energies (justified via benchmarking, see Fig. S5) at stationary point structures optimized using B3LYP/6-31+G(d) which is known to provide reliable structures. Aqueous conditions were included using an original semicontinuum (cluster + continuum) solvation approach involving appropriately microsolvated reactive species (discussed below) and the default polarizable continuum solvation model IEFPCM [6] of Gaussian09. To mimic the mechanochemistry experiment, constant external forces were applied collinearly (as usual in quantum mechanochemistry [8] and graphically illustrated by arrows in the scheme at right for the microsolvated amide solute species, see also Fig. S7) to the carbon atoms of the terminating methyl groups of a N-ethylethanamide model of the amide bond (i.e. RCONHR′ where R = Me and R′ = Et) using our in-house module [7] to rigorously carry out the isotensional (EFEI) [8] optimizations of stationary point structures (of reactants, intermediates and transition states) as a function of applied force.

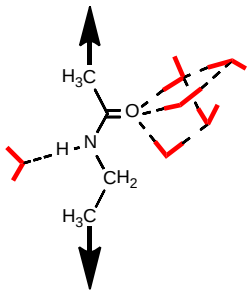

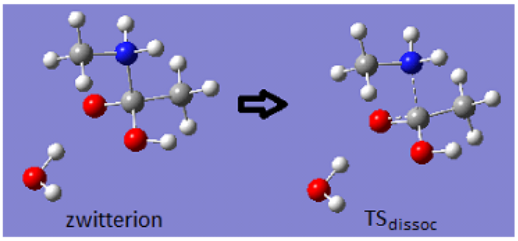

Level of theory	E(zwitterion),au	E(TS$_{dissoc}$),au	E_a (kJ mol^{-1})	basis set size
B3LYP/6-31+G(d)	-401.38686	-401.38984	-7.8	155
MP2/6-31+G(d)	-400.18210	-400.18080	3.4	155
MP2/TZVP	-400.46338	-400.46394	-1.5	199
MP2/def2-TZVPP	-400.70590	-400.70661	-1.9	371
MP2/aug-cc-pVTZ	-400.73287	-400.73264	0.6	575
CCSD(T)/6-31+G(d)	-400.26723	-400.26647	2.0	155
focal point	-400.81800	-400.81831	-0.8	

Figure S5. Benchmark test for choosing MP2/TZVP theory for computed energies. The test reaction was the activation energy (E_a) for the illustrated zwitterion dissociation reaction of $MeCOOHNH_2Me \cdot H_2O$. Energies (in au) were single-point calculations using MP2/6-31+G(d) structures. "Focal point" is the CCSD(T)/aug-cc-pVTZ estimate: E[CCSD(T)/6-31+G(d)] + {E[MP2/aug-cc-pVTZ] – E[MP2/6-31+G(d)]}.

The so-called semicontinuum approach,[9] also known as cluster + continuum modelling[10], employs a microsolvated solute species (complexed with several explicit solvent molecules) that is embedded in a continuum dielectric medium acting on the entire microsolvation complex. This computationally efficient approach improves upon both, strict microsolvation in vacuum and standard continuum modeling without explicit water by considering the proper dielectric constant (permittivity) of the far-distant solvent while simultaneously taking into account the local solute-solvent non-covalent interactions. It particularly benefits reactions involving consumption or production of H_3O^+ (and/or OH^-); it has cured a 200 kJ mol^{-1} error of the IEFPCM continuum model for the autoionization of water.[9c] This capability was found to be critical here, an OH^--catalyzed multistep reaction (cf. Scheme 1). An important aspect of semicontinuum solvation concerns the H-bond topology of the microsolvating water molecules, and for the present case of an OH^--catalyzed multistep reaction, such placement required development of a robust general methodology as follows. First, the OH^- ion was always microsolvated with m = 4 water molecules ($OH^-\cdot 4W$ m = 4 water molecules at each stage

hydroxide appears in the reaction; this choice was based on both, our prior knowledge [11] of the bulk solvation structure of OH^- (aq) and on the demonstration of $m = 4$ being both necessary and sufficient for the water autoionization energy.[9c] Second, we imposed four conservation principles to avoid artificial energy jumps between stages (stationary points) along the reaction pathway: (i) the total charge at each stage; (ii) the total number *n* of explicit water molecules (*n*W) at each stage; (iii) the total number of H-bonds (solute-solvent and solvent-solvent) formed at each stage due to placement of the *n*W, and (iv) the total number of strained HOH bond angles in the added *n*W at each stage due to the consistent use of rings of four H-bonds in the *n*W modeling (for computational tractability, to avoid difficult-to-optimize "dangling water" molecules with low-frequency internal-rotation degrees of freedom).

The conservation principles are original and deserve further comment. Conserving charge and *n*W are likely easily understood as vital for producing a connected potential energy surface profile for a multistep reaction. With regards to conserving H-bonds and HOH strain, typical artificialities that would be encountered if not avoiding these solvation artifacts are ~19 kJ mol^{-1} for H-bond imbalances, and about 11 or 6 kJ mol^{-1} for imbalances due to strained HOH angles when having two or three H-bonds, respectively (see Fig. S6).

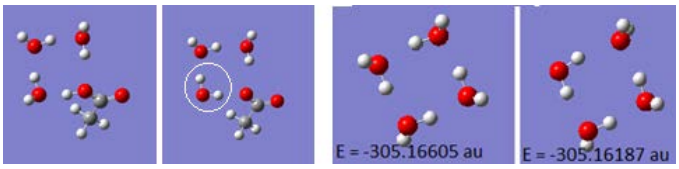

Figure S6. The two leftmost structures are examples of a four-membered H-bonded ring with minimal ring strain in case of a protonated carboxyl group, and one with a necessarily strained water molecule (circled) as a result of having deprotonated the carboxyl group. The right two panels depict water four-rings that were used to estimate the additional energy due to one strained HOH angle in a four-ring: 11 kJ mol^{-1} using our semicontiuum and electronic structure methods. Conservation of the number of such ring strains at each reaction stage was thus invoked to approximately remove these artifacts: e.g. the 16W model (see next Figure) employs 3 such strains at each stage, effectively shifting the entire potential energy surface up by an approximately constant amount.

We chose to compute solute molecules in separate semicontinua, rather than as a unified supermolecular solvation cluster at each stage (e.g. the reactant stage was RCONHR′·6W + OH^-·4W + H_2O·6W, not RCONHR′·OH^-·H_2O·16W). This was done to prevent OH^- from possibly artificially polarizing the substrate in a unified cluster.[9c] Our procedure consistently employed three independent systems at each stage of the reaction mechanism: the solvated reacting amide and two auxiliary systems serving as computational reservoirs of properly semicontinuum-solvated OH^- (aq) and H_2O(aq) species, which *together* must satisfy the conservation principles along the *entire* reaction pathway. Thus, the energies of optimized stationary points along the entire reaction pathway, either corresponding to minima or transition states at either zero or finite forces in case of the amide species, are obtained by adding the respective energies of these three systems at each step considered.

Two different semicontinuum choices (see Fig. S7 and S8), based on n = 14 and 16 water molecules in total, dubbed 14W and 16W, were developed with these semicontinuum design principles, and tested with the smaller amide-bond model N-methylethanamide (R = R′ = Me). The resulting energy profiles (Fig. S8) show a noticeable effect of the 14W versus 16W microsolvation modeling upon the energy of the *intermediates* (lowered 17 kJ mol^{-1} by 16W modelling), which can be traced back to using only two (in the 14W case) instead of three (16W) water molecules to explicitly solvate an oxygen atom that carries a -1 formal charge. However, as will be derived in the next section on the kinetics, only the energies of the two *transition states*, TS1 and TS2, relative to the reactant state, are required to solve the rate kinetics of the amide cleavage process, and these are invariant with respect to using 14W or 16W microsolvation according to the figure. All final reported results were performed with 16W and with the larger amide-bond model N-ethylethanamide (R = Me, R′ = Et).

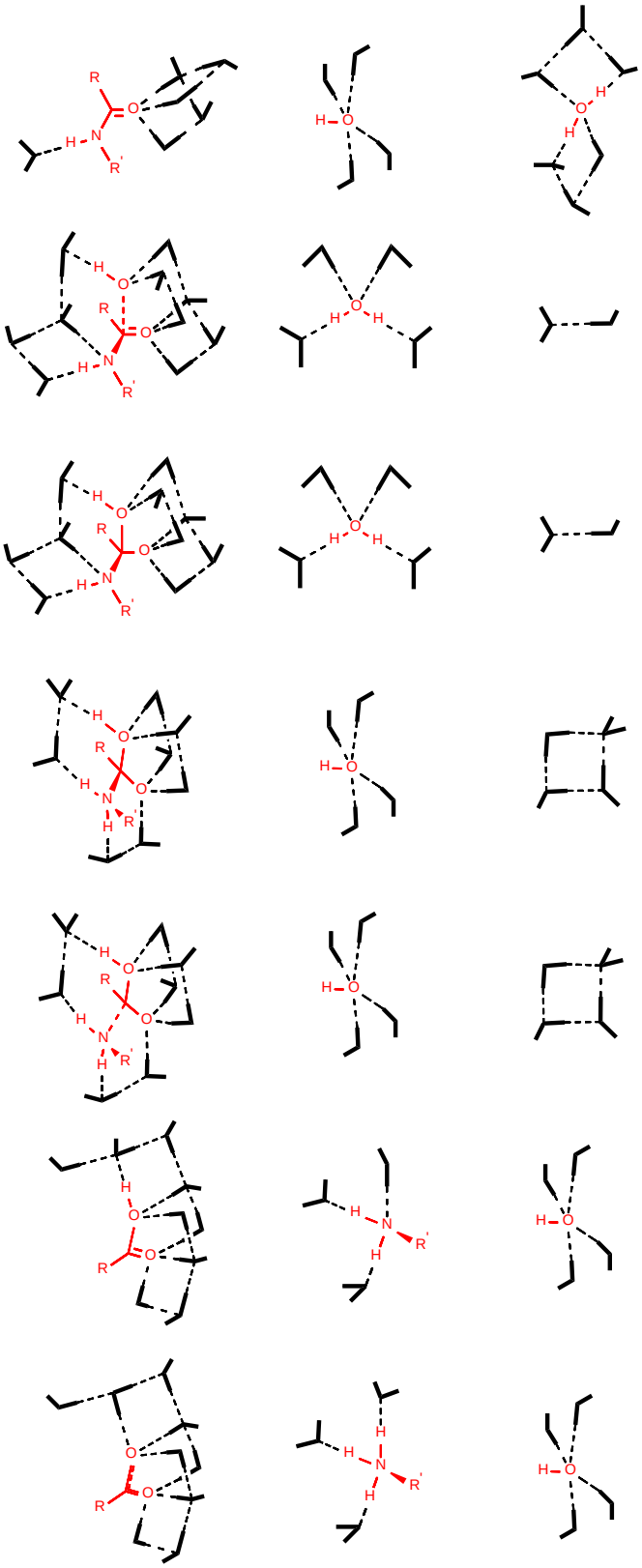

Figure S7. Schematic representation of the optimized molecular solute species (being stationary points corresponding to minima or transition states) and the two auxiliary systems, see text, using the 16W semicontinuum solvation model, see text, along the full hydrolysis pathway summarized in Scheme 1 of the main text. This shows the positions of all explicit microsolvation water molecules (bold black) and all H-bonds (dashed black). Each row is a reaction stage of Scheme 1 (corresponding to the amide, TS1, TI, ZI etc. stages), and each reaction-stage energy is the sum of the semicontinuum-computed energies of the three microsolvation complexes in the respective row. The first five microsolvated solute complexes in the first column were also optimized at various finite tensile forces, see text, in order to compute the force-dependent properties reported in Fig. 2 of the main text and needed to solve the overall kinetics to compute the effective amide bond lifetime.

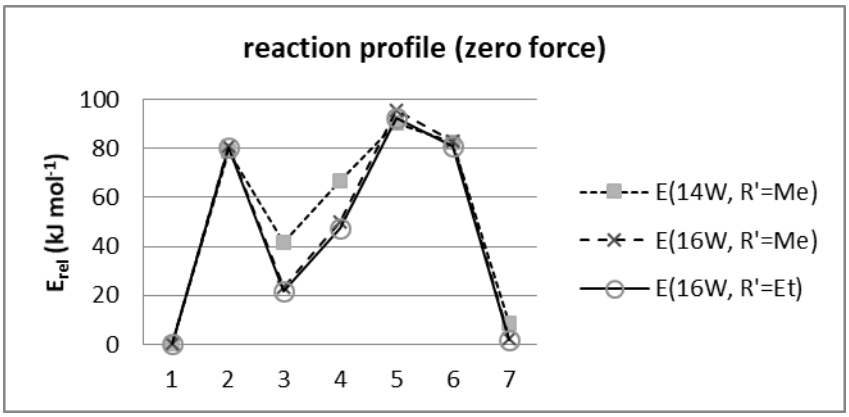

Reaction stage	14W model (17 H bonds, 2 strains)	16W model (20 H bonds, 3 strains)
amide	amide·6W + OH^-·4W + H_2O·4W	amide·6W + OH^-·4W + H_2O·6W
TS1	amide·OH^-·6W + H_2O ·4W + 4W	amide·OH^-·10W + H_2O ·4W + 2W
TI	$anion^-$·6W + H_2O ·4W + 4W	$anion^-$·10W + H_2O ·4W + 2W
ZI	$zwit^{+-}$·6W + OH^-·4W + 4W	$zwit^{+-}$·8W + OH^-·4W + 4W
TS2	acid·amine·6W + OH^-·4W + 4W	acid·amine 8W + OH^-·4W + 4W
acid + amine	acid·7W + amine·3W + OH^-·4W	acid·9W + amine·3W + OH^-·4W
carboxylate + aminium	$RCOO^-$·7W + $R'NH_3^+$·3W + OH^-·4W	$RCOO^-$·9W + $R'NH_3^+$·3W + OH^-·4W

Figure S8. Sensitivity testing of 16W vs 14W semicontinuum models: the resulting computed reaction energy profiles in the absence of tensile forces. The large amide model (R′ = Et) in conjunction with 16 water molecules was then used to compute the numbers presented in the main text. A schematic view of all systems in the 16W model is provided by Extended Data Fig. 8 where the highlighted species are also marked in red.

Computational Model: Amide Bond Lifetimes τ. The effective amide lifetime τ is the inverse of the effective rate constant k_{hyd} for the rate of hydrolysis r_{hyd} leading to cleavage of the amide bond,

$$\tau = 1/k_{hyd} \,, \qquad \ldots(S1)$$

$$r_{hyd} = -k_{hyd}\,[\text{amide}] \,, \qquad \ldots(S2)$$

where $[X]$ denotes the concentration of species X. Brown et al. [12] gives

$$k_{hyd} = \frac{k_1[\mathrm{OH^-}](k_2 + k_3[\mathrm{OH^-}])}{k_{-1} + k_2 + k_3[\mathrm{OH^-}]} \quad , \qquad \ldots(S3)$$

which results from the steady-state limit applied to the relevant mechanism,

$$\text{amide} + \mathrm{OH^-} \xrightarrow{k_1} \mathrm{TI^-}$$

$$\mathrm{TI^-} \xrightarrow{k_{-1}} \text{amide} + \mathrm{OH^-}$$

$$\mathrm{TI^-} \xrightarrow{k_2} \text{products}$$

$$\mathrm{TI^-} + \mathrm{OH^-} \xrightarrow{k_3} \text{products} .$$

This can be applied to our case because the TI/ZI equilibrium (cf. Scheme 1) is known to be fast: the transition state for this equilibrium lies much lower in free energy than those of TS1 and TS2. We will employ the usual Arrhenius equations to express the elementary rate constants in Eq. (S3),

$$k_i = A_i e^{-E_{a,i}/RT} \quad , \qquad i = \text{-1, 1, 2, 3} \qquad \ldots(S4)$$

in terms of energies which can be readily computed within semicontinuum solvation from quantum mechanochemistry as a function of constant force.

Importantly, Eq. (S3) can be simplified. First, at pH 7-10, there is no observed 2nd order term in $[\mathrm{OH^-}]$, so $k_2 >> k_3[\mathrm{OH^-}]$, which yields

$$k_{hyd} = \frac{k_1 k_2 [\mathrm{OH^-}]}{k_{-1} + k_2} \quad . \qquad \ldots(S5)$$

Second, if we insert Eq. (S4) for each k_i in Eq. (S5), write each activation energy as an energy difference (Eqs. S6a-c), i.e.

$$E_{a,1} = E_{TS1} - E_{amide+OH^-}, \quad E_{a,2} = E_{TS2} - E_{TI}, \quad E_{a,-1} = E_{TS1} - E_{TI} \quad , \ldots(S6a\text{-}c)$$

and assume similar unimolecular Arrhenius prefactors $A_{-1} = A_2$, then one can eliminate the need to know E_{TI} , and Eq. (S5) simplifies to

$$k_{hyd} = \frac{k_1 k_2' [OH^-]}{k_1 + k_2'} \quad , \qquad \ldots(S7)$$

$$k_1 = A_1 e^{-E_{a,1}/RT} \quad , \qquad E_{a,1} = E_{TS1} - E_{amide+OH^-} \quad , \qquad \ldots(S8)$$

$$k_2' = A_1 e^{-E'_{a,2}/RT} \quad , \qquad E'_{a,2} = E_{TS2} - E_{amide+OH^-} \quad . \qquad \ldots(S9)$$

Finally, inserting Eq. (S7) into Eq. (S1) results in our final expression,

$$\tau = \frac{k_1 + k_2'}{k_1 k_2' [OH^-]} \quad , \qquad (S10)$$

which we finally use to solve the coupled kinetics of the cleavage process.

The lifetimes reported in Fig. 2C were computed via Eqs. (S8-S10), employing the ab initio EFEI energies $E_{amide+OH^-}$, E_{TS1}, and E_{TS2} for the force-dependent activation energies $E_{a,1}$ and $E'_{a,2}$ (in Eqs. (S8) and (S9), plotted in Fig. 2B of the main text) which have been computed anew at each chosen value of the constant external force, and adopted the experimental estimate of the pre-exponential factor $A_1 [OH^-] = A$ from Table S2 (being approximately $A = 1 \times 10^{11}$ s^{-1}), which for simplicity is assumed to be force independent. Each EFEI energy was computed using our semicontinuum solvation approach in conjunction with the electronic structure methods and

standard dielectric continuum model for the implicit part of the solvent, using the Gaussian program package together with our in-house EFEI functionality [7-8].

Table S1. Force and temperature dependent reaction rate constants determined by AFM.

	294.15 K	298.15 K	301.15 K	303.15 K	307.15 K
F / nN	k / s^{-1}	k / s^{-1}	k / s^{-1}	k / s^{-1}	k / s^{-1}
0.6	0.0181 ± 0.0060				
0.7	0.25 ± 0.08 4.70 ±1.55				
0.8	5.86 ± 0.90	8.40 ± 0.64	7.88 ± 0.49	13.08 ± 0.80	15.24 ± 1.24
1.0	6.89± 0.85	9.07 ± 0.41	12.10 ± 0.80	13.92± 1.06	17.76 ± 0.41
1.2	9.97 ± 1.31	18.30± 1.51	14.26 ± 1.52	24.95 ± 1.51	25.02 ± 1.26
1.4	13.36 ± 1.98	19.01 ± 1.24	21.15 ± 1.66	30.22 ± 3.74	31.56 ± 1.76
1.6	20.51 ± 3.04	33.59 ± 2.53	29.08 ± 2.58	44.93 ± 4.72	50.21 ± 2.53

Table S2. Force dependent Arrhenius parameters for the first reaction step determined by AFM.

F / nN	**k_{RT} / s^{-1}**	**E_A/ kJ mol^{-1}**	**A / s^{-1}**
0.8	5.86 ± 0.90	60.8 ± 10.5	$3.3x10^{11\pm1.9}$
1.0	6.89 ± 0.85	58.1 ± 2.8	$1.3x10^{11\pm0.5}$
1.2	9.98 ± 1.31	53.0 ± 18.4	$2.8x10^{10\pm3.0}$
1.4	13.36 ± 1.98	54.4 ± 7.6	$2.8x10^{10\pm1.2}$
1.6	20.51 ± 3.04	51.4 ± 13.3	$1.5x10^{11\pm2.1}$
Extrapolation to 0 nN		69.0 ± 17.3	

References

[1] a) M. Grandbois, M. Beyer, M. Rief, H. Clausen-Schaumann, H. E. Gaub, *Science* **1999**, *283*, 1727-1730; b) S. W. Schmidt, A. Kersch, M. K. Beyer, H. Clausen-Schaumann, *PCCP* **2011**, *13*, 5994-5999.

[2] H. J. Butt, M. Jaschke, *Nanotechnology* **1995**, *6*, 1-7.

[3] a) S. W. Schmidt, T. Christ, C. Glockner, M. K. Beyer, H. Clausen-Schaumann, *Langmuir* **2010**, *26*, 15333-15338; b) S. W. Schmidt, P. Filippov, A. Kersch, M. K. Beyer, H. Clausen-Schaumann, *ACS Nano* **2012**, *6*, 1314-1321.

[4] M. J. Frisch, G. W. Trucks, H. B. Schlegel, G. E. Scuseria, M. A. Robb, J. R. Cheeseman, G. Scalmani, V. Barone, B. Mennucci, G. A. Petersson, H. Nakatsuji, M. Caricato, X. Li, H. P. Hratchian, A. F. Izmaylov, J. Bloino, G. Zheng, J. L. Sonnenberg, M. Hada, M. Ehara, K. Toyota, R. Fukuda, J. Hasegawa, M. Ishida, T. Nakajima, Y. Honda, O. Kitao, H. Nakai, T. Vreven, J. A. M. Jr., J. E. Peralta, F. Ogliaro, M. Bearpark, J. J. Heyd, E. Brothers, K. N. Kudin, V. N. Staroverov, R. Kobayashi, J. Normand, K. Raghavachari, A. Rendell, J. C. Burant, S. S. Iyengar, J. Tomasi, M. Cossi, N. Rega, J. M. Millam, M. Klene, J. E. Knox, J. B. Cross, V. Bakken, C. Adamo, J. Jaramillo, R. Gomperts, R. E. Stratmann, O. Yazyev, A. J. Austin, R. Cammi, C. Pomelli, J. W. Ochterski, R. L. Martin, K. Morokuma, V. G. Zakrzewski, G. A. Voth, P. Salvador, J. J. Dannenberg, S. Dapprich, A. D. Daniels, Ö. Farkas, J. B. Foresman, J. V. Ortiz, J. Cioslowski, D. J. Fox, Gaussian Inc, Wallingford, CT, **2010**.

[5] A. Schäfer, C. Huber, R. Ahlrichs, *J. Chem. Phys.* **1994**, *100*, 5829-5835.

[6] a) G. Scalmani, M. J. Frisch, *J. Chem. Phys.* **2010**, *132*, 114110; b) J. Tomasi, B. Mennucci, R. Cammi, *Chem. Rev.* **2005**, *105*, 2999-3094.

[7] M. Krupička, D. Marx, *J. Chem. Theory Comput.* **2015**, *11*, 841-846.

[8] J. Ribas-Arino, M. Shiga, D. Marx, *Angew. Chem. Int. Ed.* **2009**, *48*, 4190-4193.

[9] a) S. W. Rick, B. J. Berne, *J. Am. Chem. Soc.* **1994**, *116*, 3949-3954; b) K. Z. Sumon, C. H. Bains, D. J. Markewich, A. Henni, A. L. L. East, *J. Phys. Chem. B* **2015**, *119*, 12256-12264; c) S. Dhillon, A. L. L. East, *Int. J. Quantum Chem.* **2018**, *118*, e25703.

[10] J. R. Pliego, J. M. Riveros, *J. Phys. Chem. A* **2001**, *105*, 7241-7247.

[11] D. Marx, A. Chandra, M. E. Tuckerman, *Chem. Rev.* **2010**, *110*, 2174-2216.

[12] R. S. Brown, A. J. Bennet, H. Slebocka-Tilk, *Acc. Chem. Res.* **1992**, *25*, 481-488.